Endohedral Nickel, Palladium, and Platinum Atoms in 10-Vertex Germanium Clusters: Competition between Bicapped Square Antiprismatic and Pentagonal Prismatic Structures

R. B. King,*,† I. Silaghi-Dumitrescu,‡ and M. M. Uţă‡

Department of Chemistry, University of Georgia, Athens, Georgia 30602, and Faculty of Chemistry and Chemical Engineering, Babeş-Bolyai University, Cluj-Napoca, Romania

Received: July 25, 2008; Revised Manuscript Received: October 7, 2008

Density functional theory predicts significant differences in the preferred structures of endohedral $M@Ge_{10}^{z}$ (M = Ni, Pd, Pt; $z = 0, 2-, 4-$) clusters upon a change of the central metal atom in otherwise isoelectronic systems. For the neutral clusters $M@Ge_{10}$ the global minima are singlet bicapped square antiprisms. However, triplet regular pentagonal prismatic structures become increasingly energetically competitive in the series Ni → Pd → Pt. The pentagonal prismatic dianions $M@Ge_{10}^{2-}$ (M = Ni, Pd, Pt) appear to have closed shell structures and are the global minima for palladium and platinum. However, the global minimum for $Ni@Ge_{10}^{2-}$ is the capped square antiprism suggested by the Wade−Mingos rules. A number of singlet low-energy unsymmetrical structures are found for the tetraanions $M@Ge_{10}^{4-}$. However, for the palladium and platinum tetraanions triplet pentagonal prismatic structures are energetically competitive with the unsymmetrical structures.

1. Introduction

All three of the group 10 metals, namely, nickel, palladium, and platinum, have been found to occur as endohedral atoms in 10-vertex post-transition element clusters. Examples of such structurally characterized endohedral clusters include the anionic indium clusters $M@In_{10}^{10-}$ (M = Ni, Pd, Pt)[1] in the intermetallics $K_{10}In_{10}M$, the anionic lead clusters $M@Pb_{10}^{2-}$ in $[K(2,2,2\text{-crypt})]_2[M@Pb_{10}]$ (M = Ni, Pd, Pt),[2,3] and the cationic bismuth cluster $Pd@Bi_{10}^{4+}$ in $Bi_{14}PdBr_{16}$ (= $[Pd@Bi_{10}][BiBr_4]_4$).[4] In addition, group 10 metals are found as interstitial atoms in the icosahedral clusters $M@Pb_{12}^{2-}$ in $[K(2,2,2\text{-crypt})]_2[M@Pb_{12}]$ (M = Ni, Pd, Pt).[3]

The number of electrons contributed by such endohedral atoms to the skeletal bonding of polyhedral metal clusters is of interest, particularly in connection with the applicability of the Wade−Mingos rules.[5−8] In this connection the stability of the filled d^{10} shell of nickel suggests that an endohedral nickel atom might function as a pseudo noble gas and thus as a formal zero-electron donor.[9] Such appears to be the case in the nickel-centered $Ni_{10}Sb_2$ icosahedral cluster $[Ni@Ni_{10}\{SbNi(CO)_3\}_2(CO)_{18}]^{4-}$.[10] However, for the heavier group 10 elements, particularly platinum, relativistic effects[11−14] can reduce the energy separation between the d and s valence orbitals so that the $d^{10}\,s^2$ configuration rather than the d^{10} configuration is the pseudo noble gas configuration. This is suggested by the volatility of elemental mercury and its monatomic vapor as well as the existence of CsAu[15−17] and Cs_2Pt[18] containing the ions Au^- and Pt^{2-}, respectively, which have $d^{10}\,s^2$ electronic configurations isoelectronic with atomic mercury. This suggests that an interstitial platinum atom might function as a two-electron acceptor in certain cluster structures. For this reason isoelectronic clusters of the same size might be expected to have different shapes in some cases when an endohedral nickel atom is replaced by its heavier congener platinum.

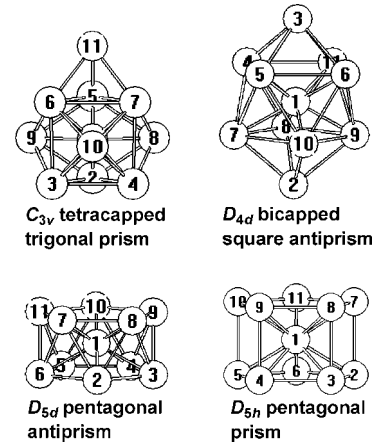

Figure 1. Initial structures used in this work.

In this study we use density functional theory (DFT) to explore the favored structures of the 10-vertex $M@Ge_{10}^{z}$ (M = Ni, Pd, Pt; $z = 0, 2-, 4-$) clusters. Germanium clusters were chosen to minimize the charge of species isoelectronic with those known experimentally. Thus, the neutral species $M@Ge_{10}$ are isoelectronic with the known[1] $M@In_{10}^{10-}$. The ionic species $M@Ge_{10}^{2-}$ and $M@Ge_{10}^{4-}$ are isoelectronic with *closo*- and *nido*-boranes, respectively, and thus provide an opportunity to test the Wade−Mingos rules.[5−8] Similar DFT calculations were also attempted on the $M@Ge_{10}^{6-}$ clusters isoelectronic with *arachno*-boranes. However, attempts to optimize the structures of $M@Ge_{10}^{6-}$ clusters led to rupture of the Ge_{10} polyhedron, possibly reflecting the instability of such species in the absence of counterions.

We previously reported a DFT study of the 10-vertex clusters $M@Ge_{10}^{z}$ containing exclusively the first-row transition metals nickel, copper, and zinc as endohedral atoms.[19] That work used a polarized (valence) double-ζ 6-31G(d) basis set for all of the atoms. Owing to the presence of the heavier transition metals palladium and platinum in this work, the effective core potential

† University of Georgia.
‡ Babeş-Bolyai University.

10.1021/jp8066074 CCC: $40.75
Published on Web 12/24/2008

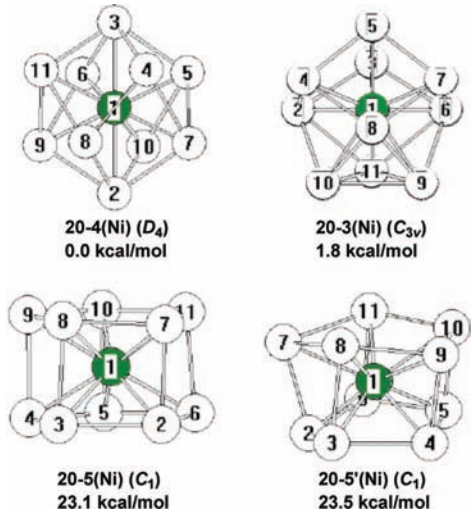

Figure 2. Optimized structures for Ni@Ge_{10}.

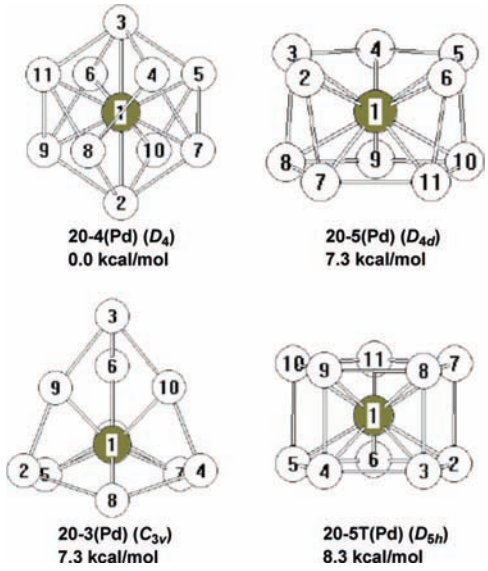

Figure 3. Optimized structures for Pd@Ge_{10}.

(ECP) LANL2DZ basis set was used to make the calculations tractable and also to include some of the relativistic effects important for these elements. To have a consistent theoretical method for all three metals, the calculations were repeated for the nickel-centered clusters using the same basis set for the endohedral atom as for the palladium- and platinum-centered clusters.

2. Computational Methods

Geometry optimizations were carried out at the hybrid DFT B3LYP level[20−23] with the ECP LANL2DZ basis set for both the interstitial and germanium atoms. The Gaussian 98 package of programs[24] was used in which the fine grid (75 302) is the default for numerically evaluating the integrals and the tight (10^{-8}) hartree stands as a default for the self-consistent field convergence. Computations were carried out using four initial geometries including 10-vertex polyhedra with 3-fold, 4-fold, and 5-fold symmetry (Figure 1). The symmetries were maintained during the initial geometry optimization processes. Symmetry breaking using modes defined by imaginary vibrational frequencies was then used to determine optimized structures with minimum energies. Vibrational analyses show

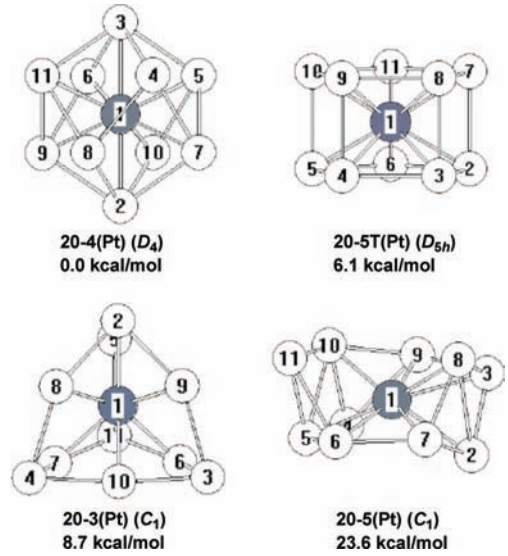

Figure 4. Optimized structures for Pt@Ge_{10}.

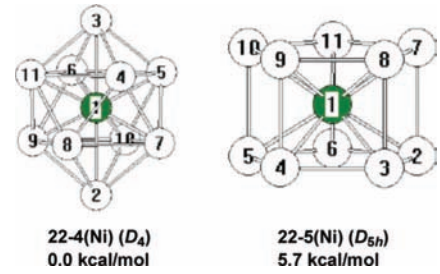

Figure 5. Optimized structures for Ni@Ge_{10}^{2-}.

that all of the final optimized structures discussed in this paper are genuine minima at the B3LYP/LANL2DZ level without any significant imaginary frequencies ($N_{imag} = 0$). In a few cases the calculations ended with acceptable small imaginary frequencies,[25] and these values are indicated in the corresponding figures.

The optimized structures found for the M@Ge_{10}^{z} clusters are labeled by the number of skeletal electrons, order of the principal rotation axis of the starting structure, and central metal atom. Triplet structures are indicated by T. Thus, the structure of singlet neutral Ni@Ge_{10} obtained from the bicapped square antiprism of D_{4d} symmetry is labeled 20-4(Ni). Additional details of all of the optimized structures, including all interatomic distances and the initial geometries leading to a given optimized structure, are provided in the Supporting Information. In assigning polyhedra to the optimized structures, Ge−Ge distances of less than ∼3.2 Å were normally considered as polyhedral edges; significant exceptions are noted in the text.

3. Results

3.1. Neutral M@Ge_{10} Structures. Figures 2, 3, and 4 show the optimized structures for the neutral M@Ge_{10} with M = Ni, Pd, and Pt, respectively. In all cases the global minima are D_4 structures derived from the bicapped square antiprism similar to the experimentally found structure[26] for the isoelectronic Zn@In_{10}^{8-} in $K_8In_{10}Zn$. The C_{3v} structure 20-3(Ni) (Figure 2) found experimentally for the Ni@In_{10}^{10-} ion in $K_{10}In_{10}Ni$ and by DFT for Ni@Ge_{10} in the previous work[19] using the 6-31G(d) basis was just 1.8 kcal/mol higher than the global minimum 20-4(Ni) using the LANL2DZ basis set. This contrasts with the observation of structure 20-3(Ni) at 4.6 kcal/mol below 20-4(Ni)

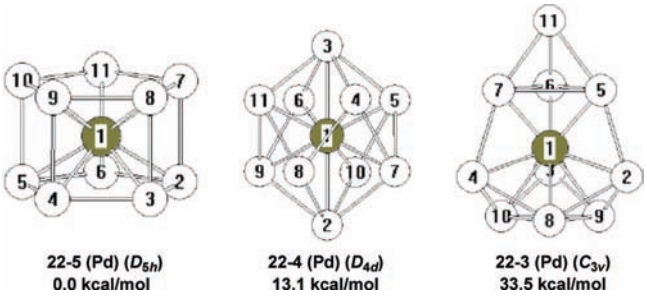

Figure 6. Optimized structures for $Pd@Ge_{10}^{2-}$.

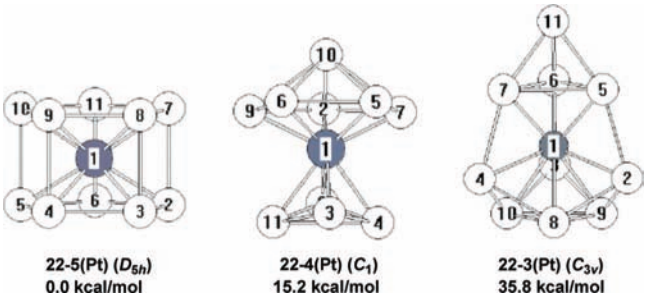

Figure 7. Optimized structures for $Pt@Ge_{10}^{2-}$.

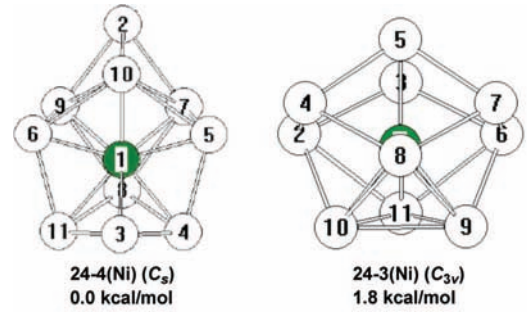

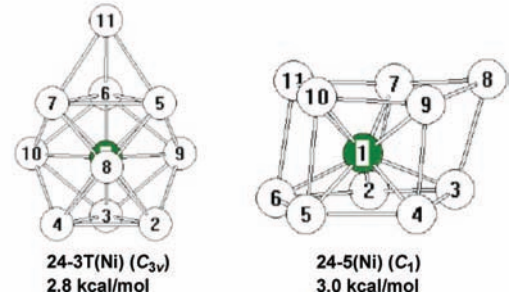

Figure 8. Optimized structures for $Ni@Ge_{10}^{4-}$.

TABLE 1: Dimensions (Å) of Bicapped Square Antiprismatic Metal Clusters

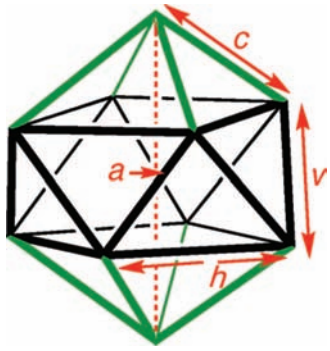

cluster	*v*	*h*	*c*	*a*	*v*/*h*	*a*/*h*
20 Skeletal Electrons						
$Ni@Ge_{10}$ [20-4(Ni)]	2.74	3.25	2.71	4.96	0.84	1.53
$Pd@Ge_{10}$ [20-4(Pd)]	2.84	3.38	2.82	5.16	0.84	1.53
$Pt@Ge_{10}$ [20-4(Pt)]	2.84	3.40	2.85	5.21	0.84	1.53
22 Skeletal Electrons						
$Ni@Ge_{10}^{2-}$ [22-4(Ni)]	2.79	3.13	2.80	5.64	0.89	1.80
$Pd@Ge_{10}^{2-}$ [22-4(Pd)]	2.88	3.29	2.88	5.65	0.88	1.72
$Pt@Ge_{10}^{2-}$ (transition state)	2.88	3.34	2.89	5.59	0.86	1.65

TABLE 2: Dimensions (Å) of Pentagonal Prismatic Metal Clusters

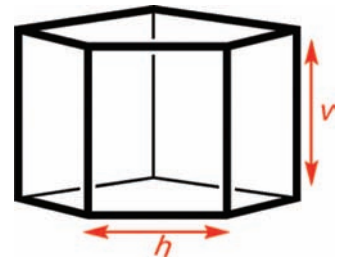

cluster	*v*	*h*	*v*/*h*
20 Skeletal Electrons			
$Ni@Ge_{10}$ (transition state)	2.63	2.60	1.01
$Pd@Ge_{10}$ [20-5T(Pd)]	2.70	2.69	1.00
$Pt@Ge_{10}$ [20-5T(Pt)]	2.71	2.71	1.00
22 Skeletal Electrons			
$Ni@Ge_{10}^{2-}$ [22-5(Ni)]	2.73	2.61	1.05
$Pd@Ge_{10}^{2-}$ [22-5(Pd)]	2.81	2.67	1.05
$Pt@Ge_{10}^{2-}$ [22-5(Pt)]	2.83	2.68	1.06
24 Skeletal Electrons			
$Ni@Ge_{10}^{4-}$ (transition state)	2.71	2.69	1.01
$Pd@Ge_{10}^{4-}$ [24-5T(Pd)]	2.75	2.77	0.99
$Pt@Ge_{10}^{4-}$ [24-5T(Pt)]	2.76	2.79	0.99

in the previous work using the 6-31G(d) (valence) ζ-quality basis functions for all atoms including the interstitial nickel atom. Structure 20-3(Ni) obtained using the LANL2DZ basis set in this work had only a small imaginary vibrational frequency at 23i and thus can be considered as a genuine minimum.

The other relatively low energy structures for $M@Ge_{10}$ are derived from the pentagonal prism. Triplet D_{5h} pentagonal prismatic structures are found for M = Pd and Pt, with the D_{5h} $Pt@Ge_{10}$ structure 20-5T(Pt) lying only 6.1 kcal/mol above the global minimum 20-4(Pt) (Figure 4). Such structures are isoelectronic with nickelocene $(\eta^5\text{-}C_5H_5)_2Ni$ by replacing the C−H bonds with the "vertical" edges of the pentagonal prism, considered as two-electron, two-center (2e−2c) bonds.

Some singlet $M@Ge_{10}$ structures (M = Ni, Pd, Pt) were found where the ideal D_{5h} pentagonal prism has undergone a Jahn−Teller distortion destroying the 5-fold symmetry. Such structures include 20-5(Ni) (Figure 2) and 20-5(Pd) (Figure 3). In addition, for $M@Ge_{10}$ (M = Pd, Pt) the relatively low lying structures 20-3(Pd) and 20-3(Pt) are found. These structures are based on a distorted tetrahedron with metal atoms at the four vertices and the six edge midpoints.

3.2. Dianions $M@Ge_{10}^{2-}$. The global minimum for $Ni@Ge_{10}^{2-}$, namely, 22-4(Ni) (Figure 5), is a bicapped square antiprism in accord with the Wade−Mingos rules[5−8] for a 22-skeletal-electron 10-vertex system ($22 = 2n + 2$ for $n = 10$). A similar structure, 22-4(Pd) (Figure 6), is found for $Pd@Ge_{10}^{2-}$ but at 13.1 kcal/mol above the global minimum. Attempts to optimize a similar structure for $Pt@Ge_{10}^{2-}$ led instead to the mushroomlike structure 22-4(Pt) in which the Ge_{10} cluster has

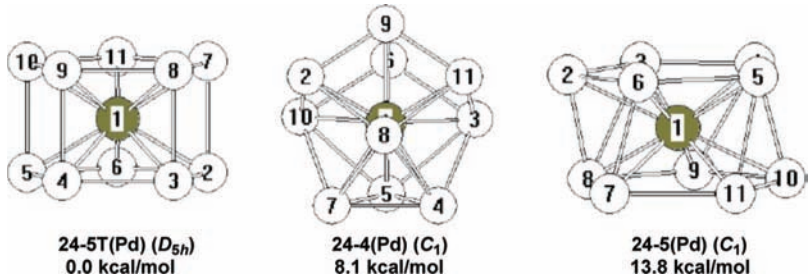

Figure 9. Optimized structures for $Pd@Ge_{10}^{4-}$.

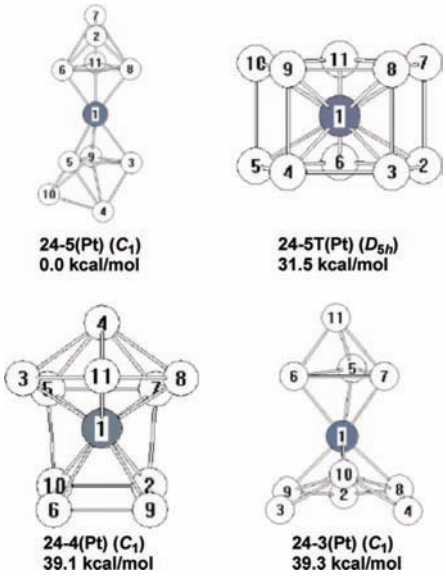

Figure 10. Optimized structures for $Pt@Ge_{10}^{4-}$.

split into a Ge_6 unit (the "cap" of the mushroom) and a Ge_4 unit (the "base" of the mushroom).

The global minima for the palladium and platinum analogues, namely, 22-5(Pd) (Figure 6) and 22-5(Pt) (Figure 7), are found to be singlet pentagonal prisms. In addition, C_{3v} structures are found for $Pd@Ge_{10}^{2-}$ and $Pt@Ge_{10}^{2-}$ but at energies more than 30 kcal/mol above the global minima (Figures 6 and 7).

3.3. Tetraanions $M@Ge_{10}^{4-}$. The lowest energy structures found for the 24-skeletal-electron systems $M@Ge_{10}^{4-}$ depend significantly on the endohedral metal atom. For nickel, the global minimum 24-4(Ni) is a polyhedron with only C_s symmetry (Figure 8). However, three other structures, namely, a singlet C_{3v} polyhedron, 24-3(Ni), a triplet C_{3v} polyhedron, 24-3T(Ni), and a distorted pentagonal prism, 24-5(Ni), lie within 3 kcal/mol of this global minimum, implying a highly fluxional system. For palladium, the global minimum 24-5T(Pd) is a triplet pentagonal prism (Figure 9). The other two $Pd@Ge_{10}^{4-}$ structures within ~13 kcal/mol of the global minimum have no symmetry. The $Pd@Ge_{10}^{4-}$ structure 24-5(Pd) is obviously a highly distorted pentagonal prism.

The global minimum for $Pt@Ge_{10}^{4-}$, 24-5(Pt), is a low-symmetry structure in which the Ge_{10} cluster splits into two nonequivalent Ge_5 units (Figure 10). The lowest lying $Pt@Ge_{10}^{4-}$ structure with an intact Ge_{10} cluster is the triplet pentagonal prism 24-5T(Pt) at a large 31.5 kcal/mol above the global minimum 24-5(Pt) (Figure 10). Structure 24-5T(Pt) is closely related to the global minimum of $Pd@Ge_{10}^{4-}$, 24−5T(Pd) (Figure 9). In the remaining two structures found for $Pt@Ge_{10}^{4-}$, namely, 24-4(Pt) and 24-3(Pt), the Ge_{10} cluster splits into Ge_6 and Ge_4 fragments (Figure 10).

4. Discussion

4.1. Bicapped Square Antiprismatic Structures. Our DFT calculations find the bicapped square antiprism to be the global minima for the neutral $M@Ge_{10}$ (M = Ni, Pd, Pt) (Figures 2, 3, and 4) as well as the dianion $Ni@Ge_{10}^{2-}$ (Figure 5). A higher energy bicapped square antiprismatic structure is found for $Pd@Ge_{10}^{2-}$ (22-4(Pd) in Figure 6). Attempts to optimize a bicapped square antiprismatic structure for $Pt@Ge_{10}^{2-}$ led to splitting of the Ge_{10} cluster into Ge_6 and Ge_4 units to give the mushroomlike structure 22-4(Pt) (Figure 7).

The optimized geometries of the bicapped square antiprismatic clusters depend on the electron count, with the dianions $M@Ge_{10}^{2-}$ being more elongated than the neutral $M@Ge_{10}$. On a more quantitative basis, the geometry of a bicapped square antiprism can be characterized by the following three different edge lengths (Table 1): (1) the lengths of the eight equivalent sides of the two square faces of the underlying square antiprism (the "horizontal" edge length, h); (2) the lengths of the eight edges connecting a vertex of one square face of the underlying square antiprism with the other square face (the "vertical" edge length, v); (3) the eight equivalent edges connecting vertices of the square faces of the underlying square antiprism with one of the two caps (the "capping" edge length, c). The elongation of the bicapped square antiprism can be measured by the v/h ratio as given in Table 1. Also the antipodal distance between the two caps of the bicapped square antiprism (a) is a good measure of the elongation or compression, which also can be defined by the ratio a/h.

Table 1 compares the dimensions of the centered bicapped square antiprismatic $M@Ge_{10}^{z}$ (z = 0, 2−) clusters studied in this work. Five of the six clusters are the genuine minima depicted in the corresponding figures. The sixth cluster, namely, $Pt@Ge_{10}^{2-}$, is not a global minimum but instead a transition state found during the optimization of square antiprismatic $Pt@Ge_{10}^{2-}$ to the mushroom 22-4(Pt) in Figure 7.

The information in Table 1 indicates a consistent correlation of v/h with the electron count. Thus, for the neutral clusters $M@Ge_{10}$ the v/h ratio is consistently 0.84, whereas for the more elongated dianions $M@Ge_{10}^{2-}$ the v/h ratio increases to 0.88 ± 0.02. The increased elongation of the dianions $M@Ge_{10}^{2-}$ as compared with the neutral $M@Ge_{10}$ is also reflected by an increase in the a/h ratio from 1.53 for the neutral clusters to 1.72 ± 0.08 for the dianions.

4.2. Structures Derived from a Pentagonal Prism. The global minima for the dianions $M@Ge_{10}^{2-}$ (M = Pd, Pt) are the singlet regular pentagonal prisms 22-5(Pd) (Figure 5) and 22-5(Pt) (Figure 6), respectively. The corresponding nickel derivative 22-5(Ni) lies only 5.7 kcal/mol above the global minimum 22-4(Ni) (Figure 4). For palladium and platinum triplet regular pentagonal prismatic structures are also found for the neutral clusters $M@Ge_{10}$ and the tetraanions $M@Ge_{10}^{4-}$ (M = Pd, Pt). In addition, the singlet structures 20-5(Ni) in

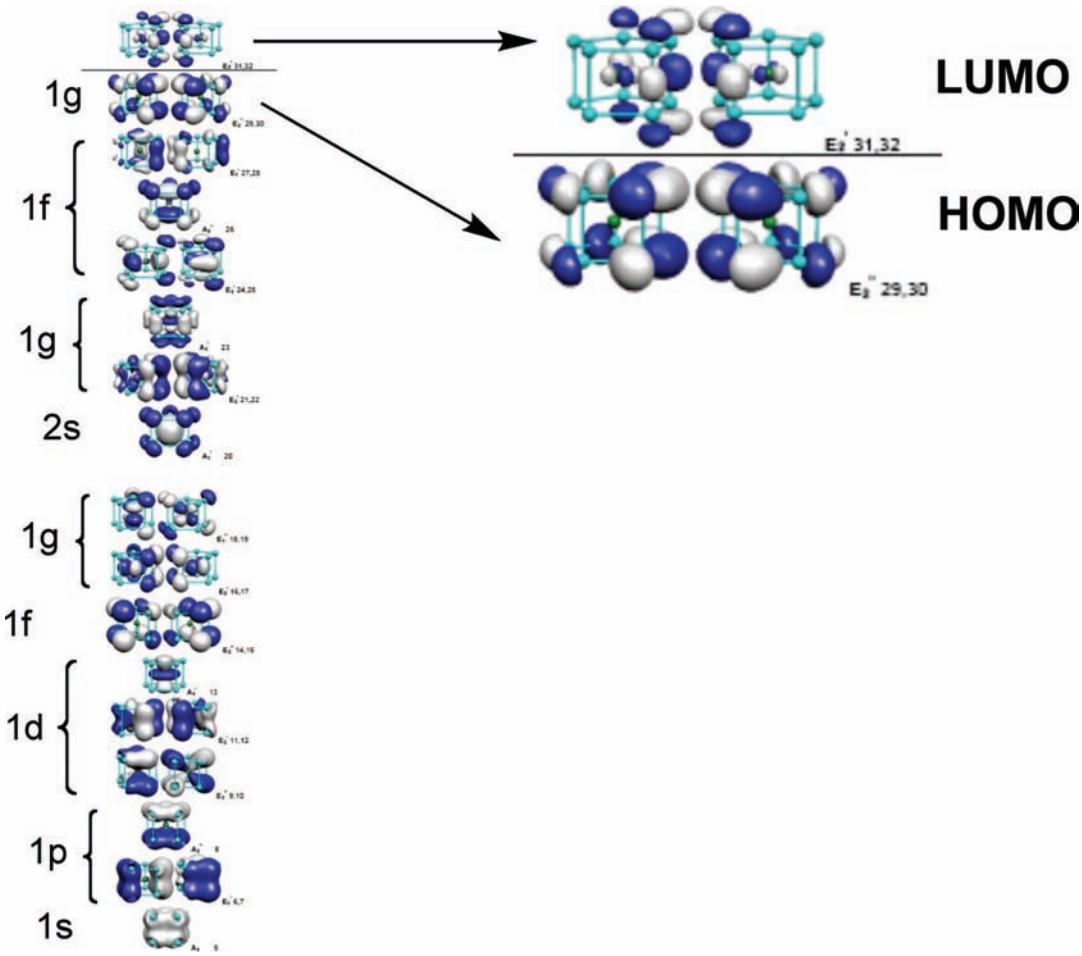

Figure 11. Bonding molecular orbitals in $Pt@Ge_{10}^{2-}$ showing the spherical harmonics of the jellium model as well as the HOMO and LUMO in greater detail.

Figure 2 and 20-5(Pd) in Figure 3 for neutral $M@Ge_{10}$ and 24-5(Ni) in Figure 8 and 24-5(Pd) in Figure 9 for the tetraanions $M@Ge_{10}^{4-}$ retain the topology of the pentagonal prism but are distorted, in most cases rather considerably, from the ideal D_{5h} symmetry of a regular pentagonal prism.

The geometry of a regular pentagonal prism can be characterized by the ratio v/h between the lengths of the vertical edges (v) and the horizontal edges (h) (Table 2). For the three singlet dianions $M@Ge_{10}^{2-}$ the v/h ratio was consistently in the range 1.05 ± 0.01 for all three metals. For the triplets, whether the neutral $M@Ge_{10}$ or the tetraanions $M@Ge_{10}^{4-}$, the v/h ratio was essentially unity, i.e., 1.00 ± 0.01. Thus, the bonding between the two pentagonal faces of the singlet dianionic $M@Ge_{10}^{2-}$ pentagonal prisms increases when two electrons are either removed to give the triplet neutral $M@Ge_{10}$ or added to give the triplet tetraanion $M@Ge_{10}^{4-}$.

The properties of the pentagonal prismatic $M@Ge_{10}^{z}$ clusters can be understood from the pattern of their molecular orbitals as depicted in Figure 11 for $Pt@Ge_{10}^{2-}$. The 52 valence electrons fill 26 bonding orbitals corresponding to a completely filled $1s^{21}p^{6}1d^{10}2s^{2}1f^{14}1g^{18}$ shell according to the jellium model used to approximate clusters by a negatively charged sphere.[27−29] This jellium model differs from the spherical model of an atom in that the balancing positive charge is distributed throughout the sphere rather than concentrated in the center such as the nucleus of an atom. This difference between the jellium sphere and the atomic sphere leads to a different distribution of the spherical harmonics including the existence of 1d, 1f, and 1g levels not found in atoms. In $Pt@Ge_{10}^{2-}$ (Figure 11) there is some intermixing of the 2s, 1f, and 1g levels, presumably owing to the deviation of a pentagonal prism from a sphere. The absence of partially filled shells for the pentagonal prismatic $M@Ge_{10}^{2-}$ clusters (M = Ni, Pd, Pt) suggests a particularly stable structure in accord with the fact that the pentagonal prisms 22-5(Pd) and 22-5(Pt) are the global minima for $M@Ge_{10}^{2-}$ (M = Pd, Pt) and the pentagonal prismatic structure 22-5(Ni) lies only 5.7 kcal/mol above the global minimum for $Ni@Ge_{10}^{2-}$.

The molecular orbital diagram shown in Figure 11 indicates that both the HOMO and LUMO are doubly degenerate for the closed shell pentagonal prismatic dianions $M@Ge_{10}^{2-}$ (M = Ni, Pd, Pt). This accounts for the fact that either removal or addition of two electrons to these dianions leads to triplets for the corresponding neutral $M@Ge_{10}$ or tetraanion $M@Ge_{10}^{4-}$ structures. In addition, this accounts for the observation of a number of singlet structures derived from an ideal pentagonal prism by Jahn−Teller distortion such as the singlet structures 20-5(Ni) in Figure 2 and 20-5(Pd) in Figure 3 for neutral $M@Ge_{10}$ as well as 24-5(Ni) in Figure 8 and 24-5(Pd) in Figure 9 for the tetraanions $M@Ge_{10}^{4-}$. Such Jahn−Teller distortions arise from splitting of the degenerate pairs of orbitals including the HOMO and LUMO.

The changes in the v/h ratios in the series $M@Ge_{10}^{z}$ ($z = 0$, 2−, 4−) of pentagonal prismatic clusters are consistent with the bonding/antibonding nature of the HOMO and LUMO orbitals as depicted in Figure 11. Thus, the HOMO of the dianions $M@Ge_{10}^{2-}$ (M = Ni, Pd, Pt) is antibonding between the two pentagonal faces of the prism (Figure 11). Removal of two electrons from this HOMO to give the corresponding neutral

TABLE 3: Metal Charges and HOMO−LUMO Gaps for $M@Ge_{10}^{z}$ Clusters

cluster	structure	relative energy (kcal/mol)	Mulliken charge on the metal M	HOMO−LUMO gap (eV)
$Ni@Ge_{10}$	20-4(Ni) (D_{4d})	0.0	−2.574	2.549
	20-3(Ni) (C_{3v})	1.8	−2.545	2.537
	20-5(Ni) (C_1)	23.1	−2.059	1.088
	20-5T(Ni) (C_1)	23.5	−2.154	1.394
$Pd@Ge_{10}$	20-4(Pd) (D_{4d})	0.0	−2.264	2.266
	20-5(Pd) (C_1)	7.3	−1.716	1.469
	20-3(Pd) (C_1)	7.3	−1.359	2.921
	20-5T(Pd) (D_{5h})	8.3	−1.842	2.356
$Pt@Ge_{10}$	20-4(Pt) (D_{4d})	0.0	−2.873	2.377
	20-5T(Pt) (D_{5h})	6.1	−2.344	2.439
	20-3(Pt) (C_1)	8.7	−1.822	2.691
	20-5(Pt) (C_1)	23.6	−1.537	2.099
$Ni@Ge_{10}^{2-}$	22-4(Ni) (D_{4d})	0.0	−2.909	2.215
	22-5(Ni) (D_{5h})	5.7	−2.262	2.133
$Pd@Ge_{10}^{2-}$	22-5(Pd) (D_{5h})	0.0	−1.980	2.237
	22-4(Pd) (D_{4d})	13.1	−2.424	1.927
	22-3(Pd) (C_{3v})	33.5	−1.486	2.071
$Pt@Ge_{10}^{2-}$	22-5(Pt) (D_{5h})	0.0	−2.394	2.338
	22-4(Pt) (C_1)	13.1	−2.491	2.103
	22-3(Pt) (C_{3v})	33.5	−1.822	2.127
$Ni@Ge_{10}^{4-}$	24-4(Ni) (C_s)	0.0	−2.934	1.904
	24-3(Ni) (C_{3v})	1.8	−3.426	1.727
	24-3T(Ni) (C_{3v})	2.8	−3.480	2.157
	24-5(Ni) (C_1)	3.0	−2.551	1.515
$Pd@Ge_{10}^{4-}$	24-5T(Pd) (D_{5h})	0.0	−1.973	1.541
	24-4(Pd) (C_1)	8.1	−2.617	1.665
	24-5(Pd) (C_2)	13.8	−2.016	1.224
$Pt@Ge_{10}^{4-}$	24-5(Pt) (C_1)	0.0	−1.351	2.444
	24-5T(Pt) (D_{5h})	31.5	−2.200	1.673
	24-4(Pt) (C_1)	39.1	−2.278	1.583
	24-3(Pt) (C_1)	39.3	−1.460	1.474

$M@Ge_{10}$ is expected to increase the bonding between the two pentagonal faces in accord with our DFT prediction of a lower v/h ratio for $M@Ge_{10}$ relative to $M@Ge_{10}^{2-}$. Similarly, the LUMO of the dianions $M@Ge_{10}$ is bonding between the pentagonal faces of the prism. Addition of two electrons to this LUMO to give the tetraanion $M@Ge_{10}^{4-}$ is expected to increase the bonding between the pentagonal faces in accord with our DFT prediction of a lower v/h ratio for $M@Ge_{10}^{4-}$ relative to $M@Ge_{10}^{2-}$.

4.3. Charge Distributions and HOMO−LUMO Gaps. Table 3 summarizes the Mulliken charges on the central metal atom M in the clusters $M@Ge_{10}^{z}$ (M = Ni, Pd, Pt; $z = 0$, 2−, and 4−). In all cases the metal atoms bear a significant negative charge. In most cases these Mulliken charges are around −2, which corresponds to a filled d^{10} s^2 shell for the central metal atom. This is the electronic configuration of mercury, which may be regarded as a pseudo noble gas,[9] as well as the Pt^{2-} anion found in the solid-state species[18] Cs_2Pt. This suggests the interpretation of these clusters as encapsulated M^{2-} anions (M = Ni, Pd, Pt), in which the bare dianion is stabilized by the surrounding Ge_{10}^{z+2} cluster. This may relate especially to the dianions $M@Ge_{10}^{2-}$. Thus, in the global minimum of $Ni@Ge_{10}^{2-}$ the central Ni^{2-} is surrounded by a Ge_{10} bicapped square antiprism. However, in the global minima of $M@Ge_{10}^{2-}$ with the larger metals Pd and Pt, the Ge_{10} polyhedron surrounding the larger M^{2-} dianions is the pentagonal prism, which has a larger volume than the bicapped square antiprism for a given edge length.

Table 3 also summarizes the HOMO−LUMO gaps for all of the $M@Ge_{10}^{z}$ (M = Ni, Pd, Pt; $z = 0$, 2−, and 4−) clusters studied in this work. A large HOMO−LUMO gap is usually associated with a particularly stable structure. In this connection the largest HOMO−LUMO gaps, which are in the range 2.7−2.9 eV, are found in the $M@Ge_{10}$ clusters 20-3 (M = Pd and Pt), in which the Ge_{10} polyhedron can be derived from a Ge_4 macrotetrahedron with additional Ge atoms at the midpoints of the six edges. The global minima for the $M@Ge_{10}$ and $M@Ge_{10}^{2-}$ clusters, namely, D_{4d} bicapped square antiprisms for the neutral $M@Ge_{10}$ (M = Ni, Pd, Pt) and the dianion $Ni@Ge_{10}^{2-}$ and D_{5h} pentagonal prisms for the dianions $M@Ge_{10}^{2-}$ (M = Pd, Pt), also have relatively high HOMO−LUMO gaps in the range 2.2−2.5 eV. In most cases the tetraanions $M@Ge_{10}^{4-}$ have lower HOMO−LUMO gaps than the corresponding dianions or neutral species.

Acknowledgment. We are indebted to the National Science Foundation for support of this work under Grant CHE-0716718. Part of this work was undertaken with financial support from the CEEX-42 SUPRAMOL program, Romania.

Supporting Information Available: Table S1, $Ni@Ge_{10}^{z}$ ($z = 6-$, 4−, 2−, 0) structures, Table S2, $Pd@Ge_{10}^{z}$ ($z = 6-$, 4−, 2−, 0) structures, Table S3, $Pt@Ge_{10}^{z}$ ($z = 6-$, 4−, 2−, 0) structures, and complete ref 24. This material is available free of charge via the Internet at http://pubs.acs.org.

References and Notes

(1) Henning, R. W.; Corbett, J. D. *Inorg. Chem.* **1999**, *38*, 3883.
(2) Esenturk, E. N.; Fettinger, J.; Eichhorn, B. *Chem. Commun.* **2005**, 247.
(3) Esenturk, E. N.; Fettinger, J.; Eichhorn, B. *J. Am. Chem. Soc.* **2006**, *128*, 9178.
(4) Ruck, M.; Dubenskyy, V.; Söhnel, T. *Angew. Chem., Int. Ed.* **2003**, *45*, 2978.
(5) Wade, K. *Chem. Commun.* **1971**, 792.
(6) Wade, K. *Adv. Inorg. Chem. Radiochem.* **1976**, *18*, 1.
(7) Mingos, D. M. P. *Nat. Phys. Sci.* **1972**, *99*, 236.
(8) Mingos, D. M. P. *Acc. Chem. Res.* **1984**, *17*, 311.
(9) King, R. B. *Dalton Trans.* **2004**, 3420.

(10) Albano, V. G.; Demartin, F.; Iapalucci, M. C.; Longoni, G.; Sironi, A.; Zanotti, V. *Chem. Commun.* **1990**, 547.
(11) Pitzer, K. S. *Acc. Chem. Res.* **1979**, *12*, 271.
(12) Pyykkö, P. *Acc. Chem. Res.* **1979**, *12*, 276.
(13) McKelvey, D. R. *J. Chem. Educ.* **1983**, *60*, 112.
(14) El-Issa, B. D.; Pyykkö, P.; Zanati, M. *Inorg. Chem.* **1991**, *30*, 2781.
(15) Sommer, A. *Nature* **1943**, *152*, 215.
(16) Spicer, W. E.; Sommer, A. H.; White, J. G. *Phys. Rev.* **1959**, *115*, 57.
(17) Dietzel, P. D. C.; Jansen, M. *Chem. Commun.* **2001**, 2208.
(18) Karpov, A.; Nuss, J.; Wedig, U.; Jansen, M. *Angew. Chem., Int. Ed.* **2003**, *42*, 4818.
(19) King, R. B.; Silaghi-Dumitrescu, I.; Uţă, M. *Chem.—Eur. J.* **2008**, 4542.
(20) Vosko, S. H.; Wilk, L.; Nusair, M. *Can. J. Phys.* **1980**, *58*, 1200.
(21) Lee, C.; Yang, W.; Parr, R. G. *Phys. Rev. B* **1988**, *37*, 785.
(22) Becke, A. D. *J. Chem. Phys.* **1993**, *98*, 5648.
(23) Stephens, P. J.; Devlin, F. J.; Chabalowski, C. F.; Frisch, M. J. *J. Phys. Chem.* **1994**, *98*, 11623.
(24) Frisch, M. J.; et al. *Gaussian 98*, revision A.11.3; Gaussian, Inc.: Pittsburgh, PA, 2002 (see the Supporting Information for the full reference).
(25) Xie, Y.; Schaefer, H. F., III; King, R. B. *J. Am. Chem. Soc.* **2000**, *122*, 8746.
(26) Dong, Z.-C.; Henning, R. W.; Corbett, J. D. *Inorg. Chem.* **1997**, *36*, 3559.
(27) De Heer, W. A. *Rev. Mod. Phys.* **1993**, *65*, 611.
(28) Janssens, E.; Neukermans, S.; Lievens, P. *Curr. Opin. Solid State Mater. Sci.* **2004**, *8*, 185.
(29) King, R. B.; Silaghi-Dumitrescu, I. *Dalton Trans.* **2008**, 6083.

JP8066074